

Time-Resolved Carrier Dynamics in Si-on-Glass Absorbers for Photovoltaic Cells

The first amorphous silicon (a-Si) photovoltaic (PV) solar cell was fabricated in 1974 (Ref. 1). By the 1980s, commercial a-Si modules were limited to about 5% efficiency² because of a light-induced degradation called the Staebler–Wronski (SW) effect, which diminishes the efficiency of a-Si cells over time due to the creation of recombination centers.^{3,4} While the impact of the SW effect could be minimized by reducing the intrinsic absorber thickness to below 250 nm, this also limited the conversion efficiency. Therefore, double-junction cells, such as a-Si–a-Si (Refs. 5 and 6) or a-Si–a-SiGe (Ref. 7), were the obvious path around the above limitations. Independently, the successful growth of microcrystalline silicon (mc-Si), a viable absorber material, was made possible by improvements in gas purification and the implementation of very high frequency (VHF) discharges. As a result, the commercialization thrust of thin-film Si PV cells has been focused on the a-Si–mc-Si tandem.⁸ Recently reported stabilized efficiencies of a-Si–mc-Si tandem cells have been as high as 11.9% as a result of cell-design optimization and the use of light-management techniques throughout the device stack.⁹ Further improvements, however, require better control of the growth process of the a-Si and mc-Si films to enhance their electron-hole recombination time, via reduced defect formation,¹⁰ improved grain-boundary passivation, and minimized unwanted contaminants.¹¹ While the empirical approach to determining the optimized deposition is preferred, it would be time consuming and cost prohibitive to use the actual completed cell characterization and analysis as a feedback mechanism. In this work, we demonstrate that a time-resolved, optical pump–probe technique provides an effective means for determining the nonequilibrium carrier dynamics for feedback on the Si growth process. We have collected a large family of normalized reflectivity change ($\Delta I/I$) waveforms of various a-Si and mc-Si films, deposited under different conditions, to determine the optimum deposition parameter space.

The basic structure of a thin-film Si tandem cell, designed in a superstrate geometry on a transparent conductive oxide (TCO)–coated glass, is shown schematically in Fig. 132.16 (Ref. 12). Presently, the most common is low-iron, soda-lime float glass with a fluorinated tin oxide as a TCO material

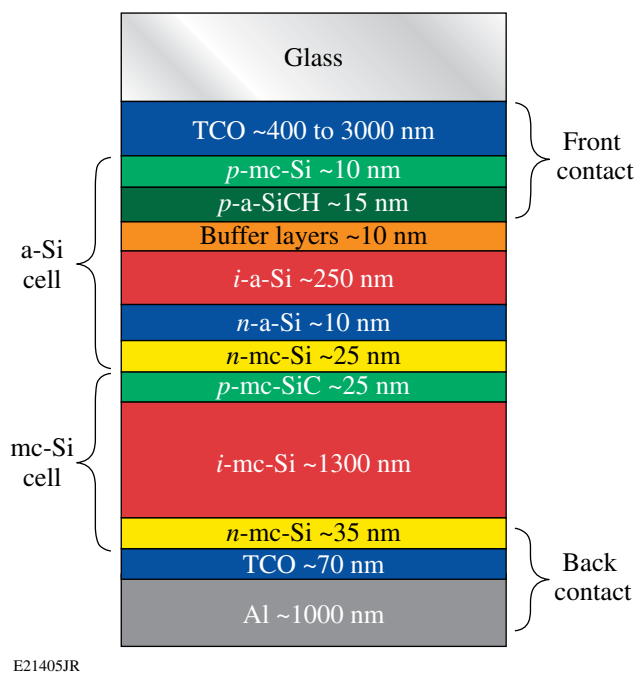


Figure 132.16
Schematic showing the layer structure of a typical Si tandem cell.

applied in-line on the float-glass process by atmospheric pressure chemical vapor deposition (APCVD).¹³ In addition, other materials, such as boron-doped, aluminum-doped, or gallium-doped zinc oxide coatings, are utilized in the Si tandem PV cells. Both the a-Si cell and the mc-Si cell are *p-i-n* structures and drift-type devices with highly doped *p* and *n* layers to set up a built-in field. Therefore, for the *i* region, the a-Si and mc-Si materials with the best-possible electron lifetime and mobility are required to ensure an efficient drift under the built-in field of the *p* and *n* contacts, particularly for the a-Si film characterization by a very low hole mobility.¹⁴

Two sets of Si-on-glass samples were deposited for this study, and the growth conditions, band gap E_G , and optical properties (complex index of refraction; n and k) are listed in Table 132.III. The first set (“S” samples) was deposited using a plasma-enhanced CVD method, and the fabricated films

Table 132.III: Deposition conditions and measured index and band gap of a-Si films used in this study. The doping type, deposition conditions [hydrogen dilution ratio, radio frequency (rf) power, and pressure], and measured index and bandgap are listed.

Sample	Type	Deposition conditions			Thickness (nm)	Spectroscopic ellipsometry measurements at 632 nm		
		Ratio (H ₂ /SiH ₄)	rf power (W)	Pressure (mtorr)		E _G (eV)	<i>n</i>	<i>k</i>
H032811S1	<i>p</i>	0.75	15	300	251.8	1.773	3.181	0.022
H032811S2	<i>n</i>	0.75	15	350	521.6	1.671	3.586	0.051
B032811S3	<i>i</i>	0.25	15	375	455.7	1.705	3.730	0.044
B032811S4	<i>i</i>	5	20	1000	342.4	1.680	3.864	0.057
B032811P3	<i>i</i>	5	20	1000	390.3	1.676	3.910	0.058
B032811P4	<i>i</i>	10	50	1000	506.9	1.818	3.651	0.015
B032811P5	<i>i</i>	1	15	1000	291.3	1.650	3.850	0.066

were primarily *p*-type SiCH and *n*-type a-Si films. Of notable interest, sample H032811S1 was deposited with a CH₄/SiH₄ ratio of 0.85 and a BF₃/SiH₄ ratio of 1. The “P” samples were deposited by the CVD method with no dopants. Intrinsic Si films grown by this system actually produced better solar cells with lower free-carrier concentration in the *i* layer. The film thickness and optical properties were determined by measuring the fringe fitting with an *n* and *k* analyzer and spectroscopic ellipsometry. The samples were 250 to 500 nm thick. Fits were performed by first fixing the optical model and surface roughness and getting thickness to fit, then fitting the material model, and finally the surface roughness. This method was required to overcome the instability inherent in the *n* and *k* fitting routines. Spectroscopic ellipsometry was performed using a commercial ellipsometer, and the data were fitted with JV’s DeltaPsi2 software.¹⁵ The a-Si was fit with the Jellison model,¹⁶ and the mc-Si was fit as a crystalline Si using the standard JV’s built-in model. Measurements were performed at a 70° angle over an energy range of 1.5 to 6.0 eV.

The carrier lifetime of our femtosecond pump–probe spectroscopy was characterized in a two-color setup using an optical system analog similar to that used by Zhang *et al.*¹⁷ The pump beam had a 400-nm wavelength and an 800-nm probe. Special care was taken to ensure proper alignment of the beams to avoid any beam “walking” since, contrary to most femtosecond pump–probe experiments, we were interested not only in the early, fastest time evolution of the photoresponse, but also in the long relaxation tail. The latter was required in order to properly resolve the Shockley–Read–Hall recombination process,^{18,19} and, correspondingly, our delay stage had a traveling range of over 30 cm. A large family of normalized transmissivity

change ($\Delta T/T$) waveforms was measured at room temperature. Each sample was tested at least three times at three different spots in order to average any film inhomogeneities. All collected transients had the same general shape and consisted of a pump-pulse–limited rising edge and a bi-exponential decay. An example, in this particular case a recorder for the S3 sample, is shown in Fig. 132.17. Based on our phenomenological fitting, the initial fast relaxation was ascribed to electron–optical phonon cooling of highly excited electrons with the corresponding characteristic time constant τ_{cool} varying from 2.4 ps and 25.7 ps for the S1 and S3 samples, respectively, to 79.2 ps for the P3 sample. We interpret the subsequent relatively slow relaxation as the Shockley–Read–Hall recombination with

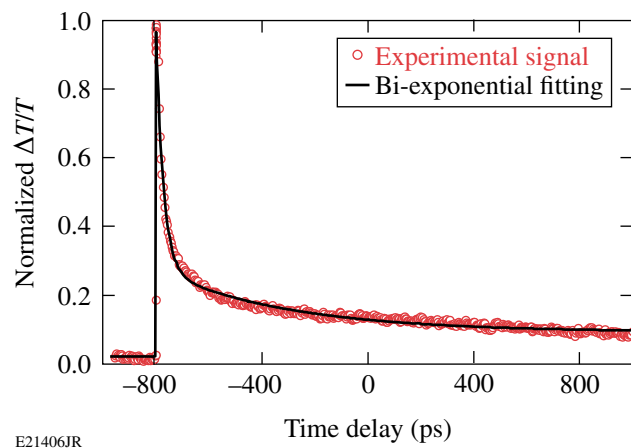


Figure 132.17 An experimental, normalized $\Delta T/T$ transient of the sample H032811S3 and a fit consisting of an error (erfc) function (rising edge) and bi-exponential relaxation (falling part).

the recombination time τ_{rec} varying from 76.4 ps and 490.5 ps for the S1 and S3 samples, respectively, to 954 ps for the P3 sample. As a result, we can see that both τ_{cool} and τ_{rec} vary substantially with the Si deposition process, with the P-type samples exhibiting the longest and most-desired τ_{rec} values.

Although the above phenomenological model provided direct indication of the desired growth conditions for maximized electron lifetime in Si PV absorbers, it did not provide physical insight into the actual carrier relaxation dynamics. It is well known that in a-Si and mc-Si materials, trapping centers strongly influence the carrier dynamics of the material.^{20–22} The early trapping model for a-Si was proposed by Tiedje *et al.* based on drift-mobility measurements.²³ The underlying concept for the model consists of a continuum of energy states instead of a discrete set. In a perfect crystal, the valence and conduction band gap edge energies are well defined. In disordered semiconductors, however, the distribution of energy states begins with transport states occupying the energy levels of the material, i.e., the conduction and valence bands. This distribution continues into the energy gap as trap states. These states form a so-called band tail, and their distribution decreases exponentially near the band edge. The widths of these exponential distributions for both the conduction and valence band tails are asymmetrical. In fact, for a-Si, the width of the valence band tail is roughly twice that of the conduction tail.^{24,25} For a-Si, the above model has been confirmed through electron photoemission^{26,27} and optical absorption²⁸ measurements.

Jepsen *et al.*²⁹ proposed a dynamical model that involves shallow trap sites in the band gap to reproduce the transient photoresponse of carriers in optically excited and pulsed THz-probed mc-Si wafers. A schematic of the proposed relaxation process is illustrated in Fig. 132.18. After absorption of a femtosecond laser pulse, the excited electrons achieve the quasi-equilibrium Fermi distribution very rapidly (within ~10 fs). Next, they lose their energy via relaxing toward the bottom of the conduction band through the electron–optical phonon interaction. After that, electrons are very likely to be trapped by the band-tail sites near the conduction-band edge. However, after all these traps are filled, the remaining photoexcited electrons are forced to directly decay to the valence band through the nonradiative electron-hole recombination, i.e., the Shockley–Read–Hall process. Independently, over time, the trapped electrons can also be released to the valence band by recombination on a time scale that cannot be distinguished from the across-the-band gap recombination time τ_{rec} . Mathematically, the above scenario corresponds to a set of linear rate equations for concentrations of photoexcited electrons (N_{hot}),

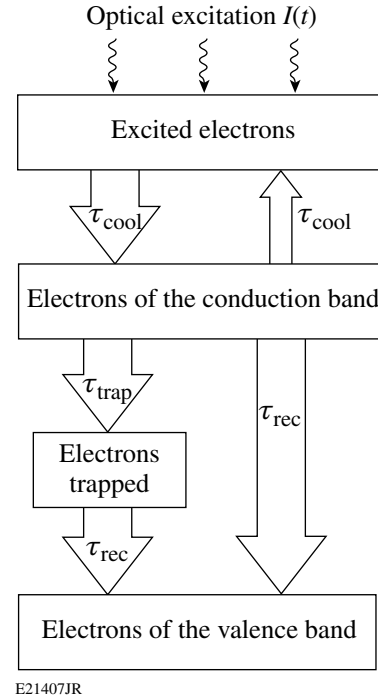


Figure 132.18

Schematic diagram of the dynamics of the carrier relaxation process for a-Si.

electrons at the bottom of the conduction band (N_{con}), and trap states N_{trap} , listed below:

$$\frac{dN_{\text{hot}}}{dt} = I(t) - \frac{N_{\text{hot}} - N_{\text{con}}}{\tau_{\text{cool}}}, \quad (1)$$

$$\frac{dN_{\text{con}}}{dt} = \frac{N_{\text{hot}} - N_{\text{con}}}{\tau_{\text{cool}}} - \left(\frac{1}{\tau_{\text{trap}}} + \frac{1}{\tau_{\text{rec}}} \right) N_{\text{con}}, \quad (2)$$

$$\frac{dN_{\text{trap}}}{dt} = \frac{N_{\text{con}}}{\tau_{\text{trap}}} - \frac{N_{\text{trap}} - N_{\text{trap,e}}}{\tau_{\text{rec}}}, \quad (3)$$

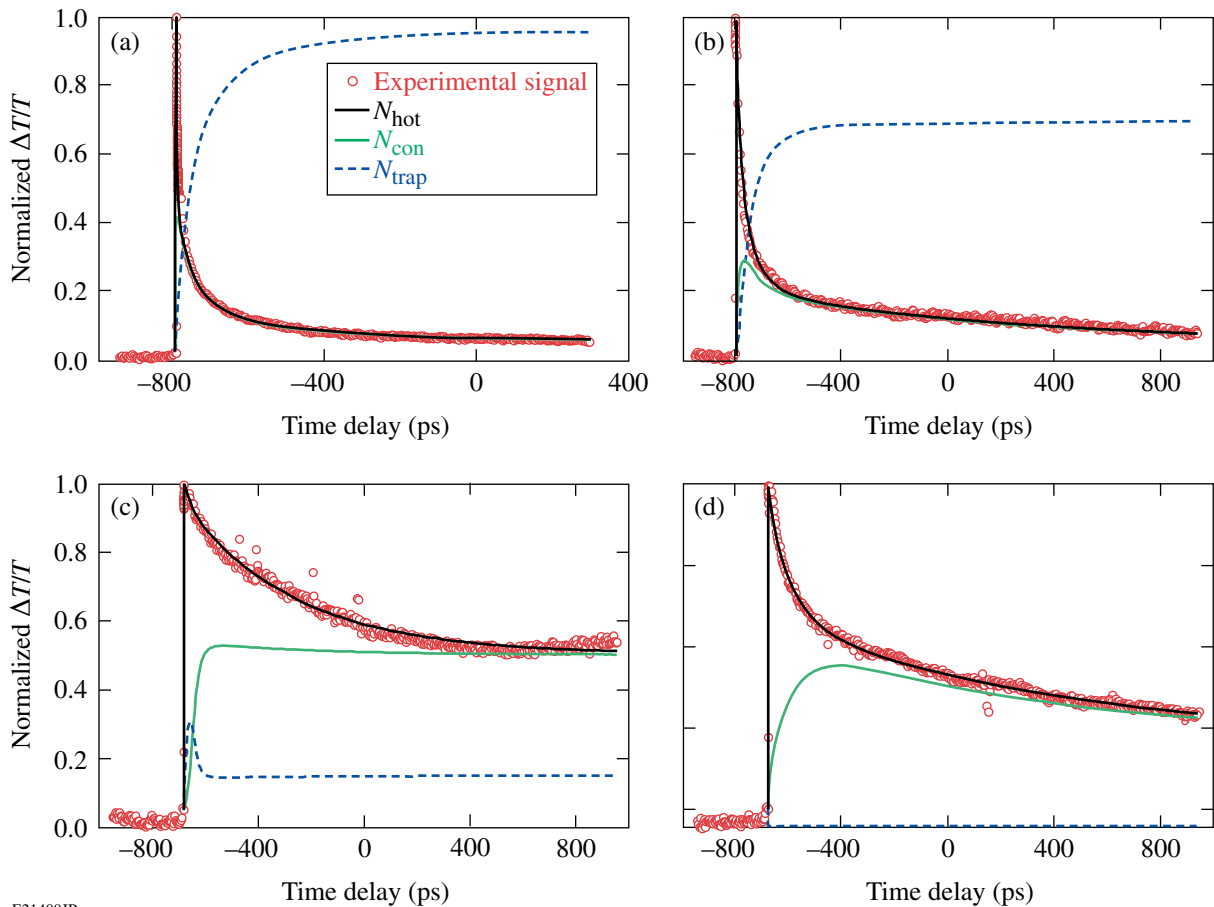
$$\tau_{\text{trap}} = \frac{\tau_{\text{trap,max}}}{1 - N_{\text{trap}}/N_{\text{trap,max}}}, \quad (4)$$

where $I(t)$ is the optical pump-pulse intensity and is assumed to be Gaussian with a width of 100 fs, τ_{trap} is the trap lifetime, and $N_{\text{trap,e}}$ is the final concentration of electrons in the trap sites. We stress that τ_{trap} actually depends on a function of the number of available trap sites and their individual lifetimes and is given by Eq. (4), with the $N_{\text{trap,max}}$ and $\tau_{\text{trap,max}}$ representing the maximum concentration of trap sites in the sample and the

longest trapping time, respectively. As compared to the equations introduced in Ref. 22, we added an extra term in Eq. (1) that is responsible for the re-exciting of some of the cooling electrons by nonequilibrium optic phonons.

Figure 132.19 shows experimental $\Delta T/T$ transients (red circles) and corresponding, simulated temporal evolutions for N_{hot} (dashed blue line), N_{con} (solid green line), and N_{trap} (solid black line) densities for four selected samples, namely, S1, S3, P5, and P3. First of all, we note that in each case the overall relaxation dynamics of photoexcited carriers, N_{hot} , fits the experimental data extremely well. At the same time, there is a considerable difference in the behavior of concentrations of trapped electrons, N_{trap} , among the various samples, providing crucial information on the difference in the density of trap sites and their trapping efficiency in samples fabricated using various methods. Figures 132.19(a) and 132.19(b) show that

in both cases (samples S1 and S3), the densities of trapped electrons are large and the trapping is clearly very efficient and effective; for the S1 sample, it reaches approximately 90% with the direct across-the-band gap recombination channel, N_{con} , representing just the background. For the S3 samples, the proportions are less dramatic, even though most of the photoexcited electrons are trapped. For these samples, traps are filled fast and remain occupied (N_{trap} almost constant) at the end of our >1-ns-wide observation window. We believe that, actually, $\tau_{\text{trap,max}}$ for these a-Si samples is very likely to be longer than the pulse repetition time of our laser (~13 ns) and in our experiments the traps are being emptied by the next incoming ultraviolet (400-nm) pump pulse. In contrast to the S-type samples, for the P5 sample [Fig. 132.19(c)], the density of trapped electrons is low, while for the P3 sample [Fig. 132.19(d)], it can be neglected. Especially in this latter case, the hot carrier dynamics N_{con} is clearly governed by the



E21408JR

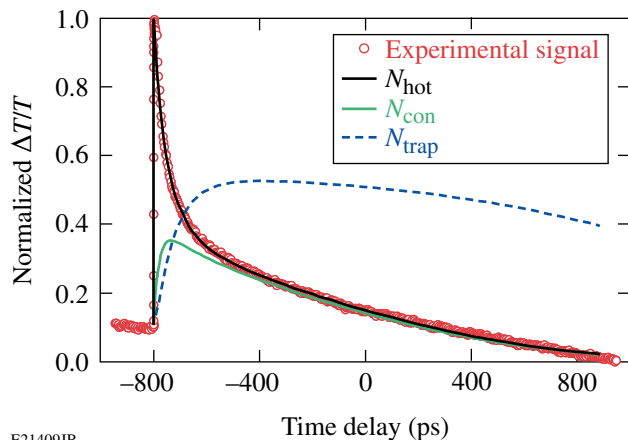
Figure 132.19

Experimental, normalized $\Delta T/T$ transients of the samples (a) H032811S1, (b) H032811S3, (c) B032811P5, and (d) B032811P3 and the corresponding simulation results based on Eqs. (1)–(4).

electron-hole recombination process, resulting in the longest value of the experimental τ_{rec} time.

The film growth conditions presented in Table 132.III corroborate with our observations. Sample H032811S1 is *p* type; therefore, its trap density is expected to be very large. The other three samples are intrinsic films with no doping; therefore, the number of trap sites should be lower. Samples B032811P5 and B032811P3 were fabricated using a growth apparatus in which the hydrogen dilution was increased as compared to the growth with the S-type samples. Since increasing hydrogen dilution shifts the material deposition from a-Si to mc-Si, we can conclude that the trap site's density has been significantly reduced in mc-Si specimens.

Finally, our S4 sample represents a very interesting case, as shown in Fig. 132.20. In this case, a significant portion of electrons is initially trapped; however, the trap lifetime is shorter than our measurement window. Therefore, we observe that at longer times, traps start to release electrons that, subsequently, “drop” to the valence band through the recombination process.



E21409JR

Figure 132.20
Experimental, normalized $\Delta T/T$ transients of the sample H032811S4 and the corresponding simulation results based on Eqs. (1)–(4).

Our femtosecond spectroscopy pump–probe experimental studies and subsequent simulations have proved that shallow trap sites in the band-tail states play a very important role in the relaxation of excited carriers in both a-Si and mc-Si samples. The relaxation dynamics reflects the trap-site densities and trapping lifetime in the samples, providing much-needed feedback on the control of wafer growth conditions. The latter is a crucial element for designing and optimizing new generations of Si-absorber-based PV solar cells with higher efficiencies.

ACKNOWLEDGMENT

This work is supported in part by the Corning, Inc., grant to the University of Rochester and by the New York State NYSTAR grant to the University of Rochester Center for Emerging and Innovative Sciences. J. Serafini acknowledges support from the Frank Horton Graduate Fellowship Program at the University of Rochester's Laboratory for Laser Energetics, funded by the U.S. Department of Energy Office of Inertial Confinement Fusion under Cooperative Agreement No. DE-FC52-08NA28302 and the New York State Energy Research and Development Authority. The support of NYSTAR and DOE does not constitute their endorsement of the views expressed in this article.

REFERENCES

1. D. E. Carlson, U.S. Patent No. 4,064,521 (20 December 1977).
2. D. E. Carlson *et al.*, *J. Mater. Res.* **13**, 2754 (1998).
3. D. L. Staebler and C. R. Wronski, *Appl. Phys. Lett.* **31**, 292 (1977).
4. P. Stradins, *Sol. Energy Mater. Sol. Cells* **78**, 349 (2003).
5. R. Platz *et al.*, *Sol. Energy Mater. Sol. Cells* **46**, 157 (1997).
6. B. Rech, C. Beneking, and H. Wagner, *Sol. Energy Mater. Sol. Cells* **41/42**, 475 (1996).
7. E. Maruyama *et al.*, *Sol. Energy Mater. Sol. Cells* **74**, 339 (2002).
9. J. Bailat *et al.*, in *25th European Photovoltaic Solar Energy Conference and Exhibition* (Valencia, Spain, 2010), pp. 2720–2723.
10. P. Torres *et al.*, in *13th European Photovoltaic Solar Energy Conference*, edited by W. Freiesleben *et al.* (Nice, France, 1995), pp. 1638–1641.
11. U. Kroll *et al.*, *J. Vac. Sci. Technol. A* **13**, 2742 (1995).
12. J. Müller *et al.*, *Sol. Energy* **77**, 917 (2004).
13. C. Beneking *et al.*, *Thin Solid Films* **351**, 241 (1999).
14. R. Brenot *et al.*, *Thin Solid Films* **383**, 53 (2001).
15. DeltaPsi2 ©2006, HORIBA Jobin Yvon, Inc., Edison, NJ 08820-3012.
16. G. E. Jellison, Jr., M. F. Chisholm, and S. M. Gorbatskin, *Appl. Phys. Lett.* **62**, 3348 (1993).
17. J. Zhang, A. Belousov, J. Karpiński, B. Batlogg, G. Wicks, and R. Sobolewski, *J. Appl. Phys.* **110**, 113112 (2011).
18. R. N. Hall, *Phys. Rev.* **87**, 387 (1952).
19. W. Shockley and W. T. Read, Jr., *Phys. Rev.* **87**, 835 (1952).
20. S. Brehme *et al.*, *Mater. Sci. Eng. B* **69–70**, 232 (2000).
21. W. Fuhs, P. Kanschä, and K. Lips, *J. Vac. Sci. Technol. B* **18**, 1792 (2000).
22. E. A. Schiff, *J. Phys.:Condens. Matter* **16**, S5265 (2004).

23. T. Tiedje *et al.*, Phys. Rev. Lett. **46**, 1425 (1981).
24. X. Deng and E. A. Schiff, in *Handbook of Photovoltaic Science and Engineering*, edited by A. Luque and S. Hegedus (Wiley, Chichester, England, 2003), Chap. 12, pp. 505–566.
25. Q. Gu *et al.*, Phys. Rev. B **52**, 5695 (1995).
26. L. Ley, J. Non-Cryst. Solids **114**, 238 (1989).
27. W. B. Jackson *et al.*, Phys. Rev. B **31**, 5187 (1985).
28. G. D. Cody *et al.*, Phys. Rev. Lett. **47**, 1480 (1981).
29. P. Uhd Jepsen *et al.*, Appl. Phys. Lett. **79**, 1291 (2001).